Growth of multi-layered graphene on molybdenum catalyst by solid phase reaction with amorphous carbon

Ricciardella, Filiberto; Vollebregt, Sten; Kurganova, Evgenia; Giesbers, A.J.M.; Ahmadi, Majid; Sarro, Pasqualina Maria

Important note
To cite this publication, please use the final published version (if applicable).
Please check the document version above.

PAPER

Growth of multi-layered graphene on molybdenum catalyst by solid phase reaction with amorphous carbon

View the article online for updates and enhancements.

IOP ebooks™

Bringing you innovative digital publishing with leading voices to create your essential collection of books in STEM research.

Start exploring the collection - download the first chapter of every title for free.

2D Materials

PAPER

Growth of multi-layered graphene on molybdenum catalyst by solid phase reaction with amorphous carbon

Filiberto Ricciardella[1] , **Sten Vollebregt**[1] , **Evgenia Kurganova**[2], **A J M Giesbers**[3], **Majid Ahmadi**[4] and **Pasqualina Maria Sarro**[1]

1   Department of Microelectronics, Delft University of Technology, Feldmannweg 17, 2628 CT Delft, The Netherlands
2   ASML, De Run 6501, 5504 DR Veldhoven, The Netherlands
3   Philips Innovation Services, MEMS & Micro Devices, High Tech Campus 4, 5656 AE Eindhoven, The Netherlands
4   Kavli Institute of NanoScience, Delft University of Technology, Mekelweg 2, 2628 CD Delft, The Netherlands

E-mail: filiberto.ricciardella@gmail.com **and** s.vollebregt@tudelft.nl

Abstract

A method to grow multi layers graphene (MLG) just by thermal annealing in an inert atmosphere is reported. A molybdenum (Mo) catalyst layer is used in combination with a solid amorphous carbon (a-C) source on top or below the Mo layer.

The formation of MLG directly on top of the catalyst substrate surface is confirmed by Raman spectroscopy, atomic force microscopy, cross-section transmission electron microscopy, electron energy loss spectroscopy and x-ray photoelectron spectroscopy. Growth of MLG on top of the Mo catalyst is demonstrated both with a-C below and above the Mo layer. The growth mechanism is attributed to the diffusion of a-C through the Mo layer and precipitation into the graphene at the surface, similar to the growth by chemical vapour deposition (CVD) on a Ni catalyst. The role of the inert Ar/H_2 atmosphere, carbon thickness, catalyst thickness, anneal time and anneal temperature are reported. Fast growth of MLG (5 min) at 915 °C is demonstrated. The quality of MLG prepared by thermal annealing is at least as good as that of MLG synthesized by CVD. The relevant achievements presented in this study make the proposed technique a promising alternative to CVD based MLG.
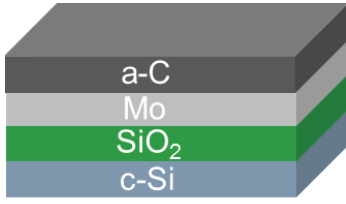
1. Introduction

Since the discovery of graphene, several approaches to produce high quality material have been explored. Currently, the best techniques for industrial scale production are liquid phase exfoliation, epitaxial growth on SiC, electrochemical methods and chemical vapor deposition (CVD) [1–5]. CVD represents the most inexpensive and promising route suitable to combine high quality and purity graphene with large scale production, especially relevant for applications within semiconductor technology [6, 7].

In the conventional CVD process, graphene growth requires carbon supersaturation at the catalyst interface, usually at around 1000 °C [8]. Typical catalyst materials are transition metals, such as Cu, Co, Ni, Pt, Pd [9]. Among the possible catalysts, Cu is proved to be the best candidate for uniform single layer of graphene growth. Integration in a wafers based process, however, suffers from several disadvantages making Cu not the

optimal catalyst choice. The low melting point causes deformation of the Cu thin film, while the thermal expansion coefficient mismatch with the silicon wafers creates large stresses and can induce roughness. Finally, Cu is an undesired element in most active devices. For few or multi-layered graphene (MLG), Ni is often used as a catalyst. Nichel is however known to result in graphene layers with a large thickness variation at the microscale. A better suitable material for wafer integration is molybdenum (Mo). Mo was shown to give good and uniform graphene growth [9, 10] and is CMOS compatible. It has a high melting point ($\sim$2600 °C), a thermal expansion coefficient closer to that of Silicon (Mo = 4.8 versus Si = 2.6 $\mu m \cdot m^{-1} \cdot K^{-1}$) than Ni and Cu. Finally, Mo is easy to remove in common etchants such as H_2O, H_2O_2 and HNO_3, making integration with CMOS easier.

Up to now, graphene growth by CVD has been prevalently focused on obtaining the crystal nucleation starting from the hydrocarbon gas sources, such

Table 1. Layer stacks of Mo and a-C with respective thicknesses. In the last column, the sketches of the base structures are displayed.

Sample	Layer 1	Thickness (nm)	Layer 2	Thickness (nm)	Schematic of layer stacks
Sample 1	a-C	500	Mo	20	
Sample 2	a-C	40	Mo	20	
Sample 3	Mo	50	a-C	500	
Sample 4	Mo	50	a-C	40	

as methane, acetylene, ethylene, benzene or hexane [6, 11], as well as liquid precursors, such as ethanol, methanol, 1-propanol or liquid hexane [6, 7, 11–14].

Only a few attempts for starting from solid state carbon precursors have been reported so far [15–17]. In particular, graphene growth has been demonstrated underneath thin-films catalyst [16, 17]. Other new methods for the synthesis of carbon nanomaterials, such as the chlorination of amorphous and 2D crystalline carbide, and the synthesis directly from an indecomposable solid carbon source, have been recently explored [18–22].

In this work, we present graphene grown on top of Mo from a solid amorphous carbon (a-C) precursor layer. We show MLG nucleation by using a solid phase reaction assisted only by annealing at 915 °C. We demonstrate that the proposed process generates high quality MLG on both stacks of Mo underneath or above the a-C layer.

2. Experimental sections

2.1. Material preparation

Silicon (1 0 0) wafers (p-type) with resistivity of 20–30 Ωcm covered by a 500 nm-thick thermally grown SiO_2 film were used as base substrate. On top of the oxided Si wafers, a double layer, either Mo on top of a-C or a-C on top of Mo, was deposited (see table 1 for details). The Mo and a-C layers were sputtered in a Veeco Nexus cluster tool at room temperature from targets having purity equal to 6N5 and 4N for Mo and C, respectively.

To grow graphene, we performed a thermal anneal up to 915 °C in an AIXTRON BlackMagic Pro. The anneal gas consisted of an Ar and H_2 mixture at a pressure of 25 mbar. The temperature profile for the annealing process is illustrated in figure 1.

The temperature profile starts with a three stages slow ramp up to 915 °C in order to reduce thermal stress in the Si and Mo layers.

The first stage is the fastest one with a rate of 200 °C min^{-1}, rising from room temperature to 525

°C. It is followed by a slower ramp rate (50 °C min^{-1}) till 725 °C. For the third stage, the ramp up rate is 30 °C min^{-1} and lasts until the final temperature (915 °C) is reached. A 1 min interval for temperature stabilization is included between the different ramp up stages. The growth is performed at 915 °C for different time windows, as summarized in table 2.

The cooling down rate is 25 °C min^{-1} till 525 °C. At this point, the heater is completely switched off. Because of the thermal inertia, the cooling down has an exponential profile, as shown by the black line in figure 1.

The annealing was carried out in a mixture of Ar and H_2. By varying the ratio of the two gases and/or the growth time, the influence of the gas atmosphere on the growth process (see table 2) was investigated.

In figure 2 the different initial layer stacks are depicted in panels (a) and (b), with a-C underneath and above the catalyst layer, respectively.

The panels (c) and (d) schematically display the evolution of the layers in panels (a) and (b), respectively, due to the annealing process. The details of the physical growth process are addressed in the section 3.

2.2. Material characterization

Samples were investigated with Raman spectroscopy before and after the annealing step. We used a Renishaw inVia Reflex spectrometer equipped with a 633 nm He–Ne laser in the back-scattering configuration. The measured output power of the laser was around 2.3 mW using a 50 × objective with a numerical aperture of 0.50. The spectra were captured on three different points of the sample. The test samples have an area of roughly 4 cm^2 cut out of the original 10 cm diameter wafers.

The surface morphology of the samples after growth was measured by atomic force microscopy (AFM) employing a ND-MDT AURA set-up, operating in semi-contact mode with a poly-Si HA-NC cantilever having a radius <10 nm, at a rate of 0.60 Hz and acquiring 256 lines on scanned areas of 25 μm^2.
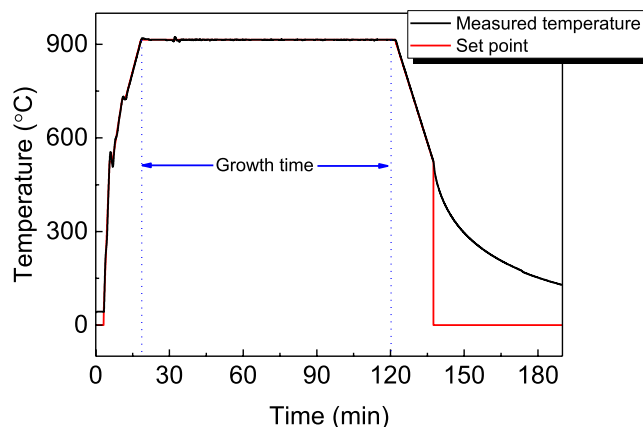
Figure 1. Process cycle of graphene growth displaying both set (red line) and measured (black line) temperature profiles as a function of time.

X-ray photoelectron spectroscopy (XPS) was employed to investigate the formation of the Mo_2C during the anneal process. The XPS measurements were carried out in a Quantera SXM™ from ULVAC-PHI using monochromatic AlKα-radiation (25 W) and a take-off angle Θ of 45°. Concentration depth profiles were determined by alternating measurements and Ar ion bombardment, using 2 or 4 keV energy.

After growth, a FEI image corrected Titan Cube 80–300 kV delivers a cross-sectional analysis of the samples. Lamellae of about 12 μm for transmission electron microscopy (TEM) were prepared using a dual-beam Helios G4 CX focused ion beam-scanning electron microscope (FIB_SEM). To protect the area of interest (AOI), a thin layer of Pt was deposited on the AOI using electron beam induced deposition (EBID) method. To protect the sample during the TEM lamella preparation process, another layer of Pt of about 1200 μm was deposited using ion beam induced deposition (IBID).

3. Results and discussion

Figure 3 displays the Raman spectra captured on the substrates described in table 1. The top two panels (*Sample 1* and *Sample 2*, figures 3(a)–(d)) show the Raman spectra on the Mo on a-C stacks. The bottom two panels *(Sample 3 and Sample 4*, figures 3(e)–(h)) refer to a-C on top of Mo stacks. In each panel, the spectra on the left side are recorded before the thermal anneal. The spectra on the right side show the results of the thermal anneal following *Recipe #1* from table 2.

The spectra on the left side of each panel display a broad band around 1500 cm^{-1} typical for amorphous carbon with a clear absence of any large-scale crystalline order [15, 16]. This band originates from the convolution of the defect related D-band, typically found at 1330 cm^{-1} for the used laser wavelength, and the sp^2-carbon G-band at 1580 cm^{-1} [23]. The broad band is more evident in figures 3(e) and (g). On the two samples with the metallic Mo layer on top (figures 3(a) and (c)), the Raman signals are partly quenched by the

Table 2. Recipes for graphene growth.

Recipe	Growth temperature (°C)	Growth time (min)	Composition of Ar/H_2 atmosphere (sccm)
1	915	90	960/40
2	915	60	960/40
3	915	30	960/40
4	915	90	0/1000
5	915	60	0/1000
6	915	30	0/1000
7	915	90	1000/0

thin metal layer but are still clearly representative of an amorphous carbon layer.

The Raman spectra provide insight on the role of the solid precursor thickness on the growth process. The Raman spectra of all samples change after the anneal step. *Sample 1, Sample 3* and *Sample 4* present a graphitic signal whilst *Sample 2* does not show any detectable signal even though the layers stack is similar to *Sample 1*. The only difference between *Sample 1* and *Sample 2* as well as between *Sample 3* and *Sample 4* is the thickness of the a-C layer (see table 1). These observations lead to conclude that the thickness of the solid precursor plays an important role in both the growth process and the final graphitic structure.

After the anneal, all samples with the exception of *Sample 2* exhibit the D-band (~1330 cm^{-1}) and G-band (~1580 cm^{-1}). Compared to the overall absence of any lattice structure, argued from the spectra in figures 3(a)–(g), the splitting of the singular peak into two clear separate bands indicates a hexagonal sp^2 structure, although disordered to some extent [16, 23, 24]. *Sample 1* and *Sample 4* also present the sharp 2D peak at around 2700 cm^{-1}, typically associated to the graphite-like materials. For *Samples 1* and *Sample 4*, the average full width half maximum (FWHM) measures 45 and 59 cm^{-1}, respectively. Hence, the rise of the 2D peak having a FWHM of a few tens of cm^{-1} and the presence of D and G-peaks definitely prove the graphitization on the structures [25].
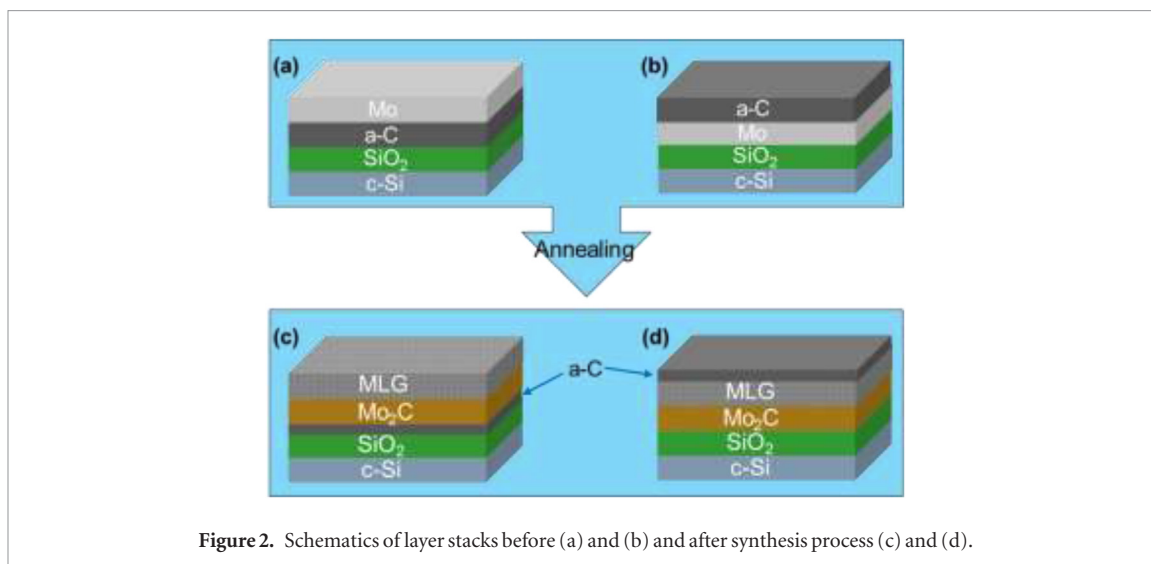
Figure 2. Schematics of layer stacks before (a) and (b) and after synthesis process (c) and (d).
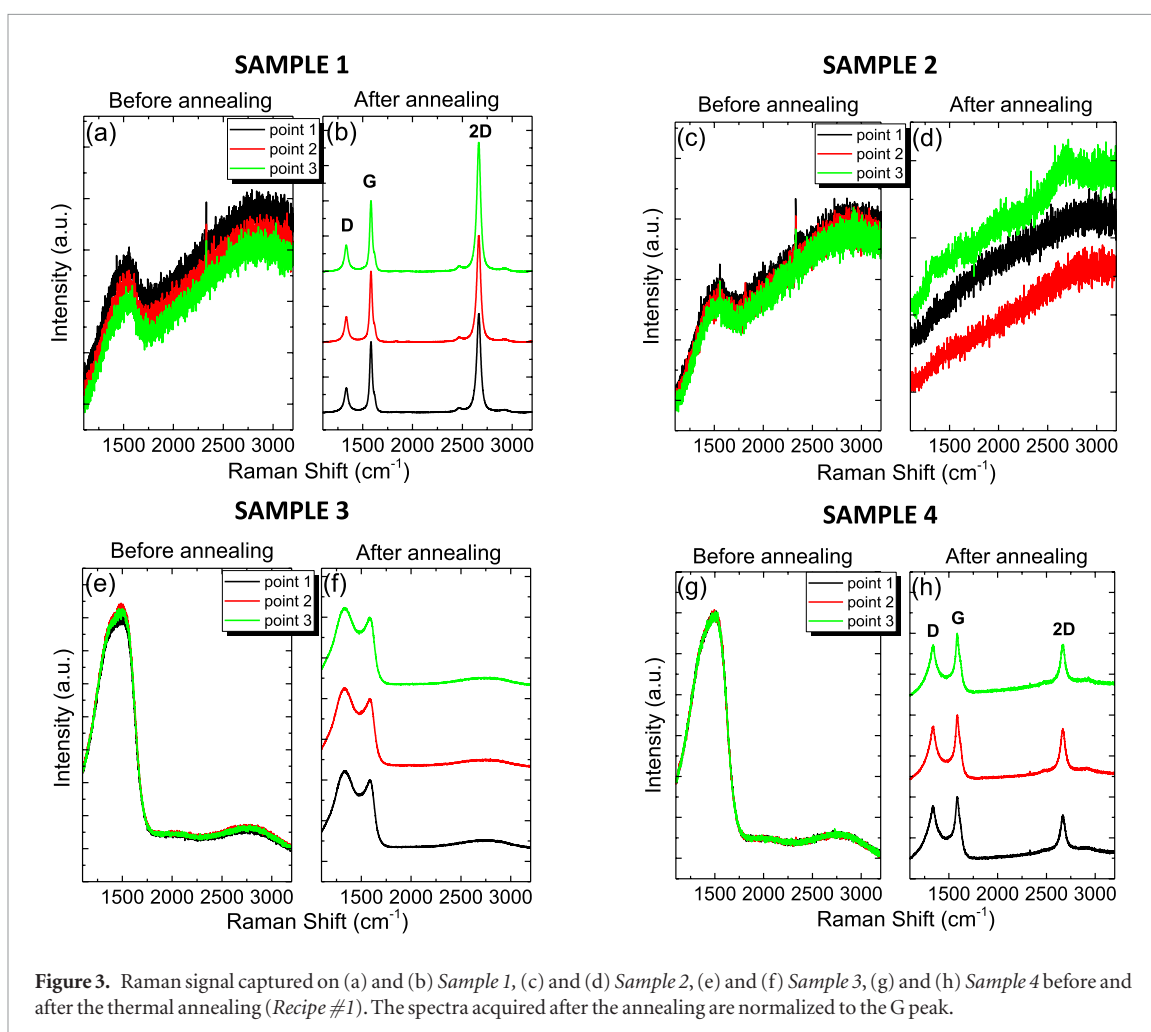
Figure 3. Raman signal captured on (a) and (b) *Sample 1,* (c) and (d) *Sample 2,* (e) and (f) *Sample 3,* (g) and (h) *Sample 4* before and after the thermal annealing (*Recipe #1*). The spectra acquired after the annealing are normalized to the G peak.

Noteworthy, the graphene-like signal on *Sample 1* (figure 3(a)) and *Sample 4* (figure 3(c)) demonstrates that a solid a-C source can be used to grow MLG. Somewhat surprisingly, the a-C can be located either underneath or above Mo film. At the same time, *Sample 3* (figure 3(b)) displays how the stack details do affect the growth. A thick top carbon layer only results in the D and G bands splitting, indicative of the transition from a disordered structure to an arranged structure [23]. No clear graphitic structure is formed as this would have resulted in a 2D band.

Further insight in the material structure is provided by STEM (scanning transmission electron microscopy) and cross-sectional TEM (transmission electron microscopy) investigation on the lamellae prepared as described in the experimental section. Images acquired in different spots of the samples are reported in figure 4.

STEM and TEM images (figures 4(a)–(b)) show the overall structure of the sample just sketched in figure 2(c). Both images display the modifications of the initial layers of Mo and a-C. The a-C layer diffused inside the Mo film over the entire sample. This diffusion assisted by the elevated temperature formed Mo_2C which is visible as the darker structures about 70 nm thick (figures 4(b) and (c)). Mo_2C formation, discussed in more details in the supporting information (figure S1 (stacks.iop.org/TDM/6/035012/mmedia)), has been demonstrated by Gall and his group [26] and also recently during the growth on Mo by CVD [27]. In our case, once Mo_2C was formed, the Mo broke up into nanocrystals, likely due to the low thickness of the initial Mo film (20 nm). Some of the Mo_2C particles migrated through the entire a-C layer leaving graphitic planes in the wake [28]. The particles are clearly visible in figure 4(b) (see red circles). The migration of the Mo_2C particles is even clearer in figure 4(c), where some facets of Mo_2C formed inside the a-C layer are shown. The paths left along the wake during the migration of the Mo_2C particles are again visible, sometimes appearing as needlelike Mo_2C crystallites. A similar phenomenon, called metal-induced lateral crystallization, is encountered in the field of semiconductors [29].

The breakdown of the Mo film can be ascribed to the thin catalyst layer, being only 20 nm. We investigated a sample having a thicker Mo layer (100 nm) and we found no disruptions in the Mo film, regardless the unchanged capability to grow MLG (figure S2).

On top of the Mo_2C (figure 4(c)), a graphitic layer was formed either during the anneal or after the segregation of C during the cooling phase. As claimed by Nakajima and co-authors, most likely the formation of the graphitic layer occurred during the annealing process [17]. a-C diffuses into Mo the layer and once the supersaturation of C is reached, the stable graphitic structures start nucleating on top of the formed Mo_2C.

Figure 4(d) is the close-up of the red square in figure 4(c). Above the Mo_2C facets, two parts roughly separated by the yellow dashed line are visible (figure 4(d)). The portion below the line is characterized by clearly distinguishable fringes, having a thickness of about 10–15 nm. The fringes can be uniquely assigned to the grown MLG, as previously highlighted by the Raman spectra (figure 3(b)). The number of graphene layers is estimated to be 20–30, assuming the thickness of a single layer to be 0.4–0.5 nm [30]. Above the yellow line, no ordered structures are recognized. The amorphous material might come out from the amorphous Pt produced by the FIB during the lamella preparation (see Experimental part). The presence of MLG is confirmed by electron energy loss spectroscopy (EELS). The inset in figure 4(d) reports the EELS spectra taken on *Sample 1*. The appearance of the peak at around 290 eV (red curve), which is not present in the a-C spectrum (black curve), definitively demonstrates the transition from a-C to a graphite structure [31, 32].
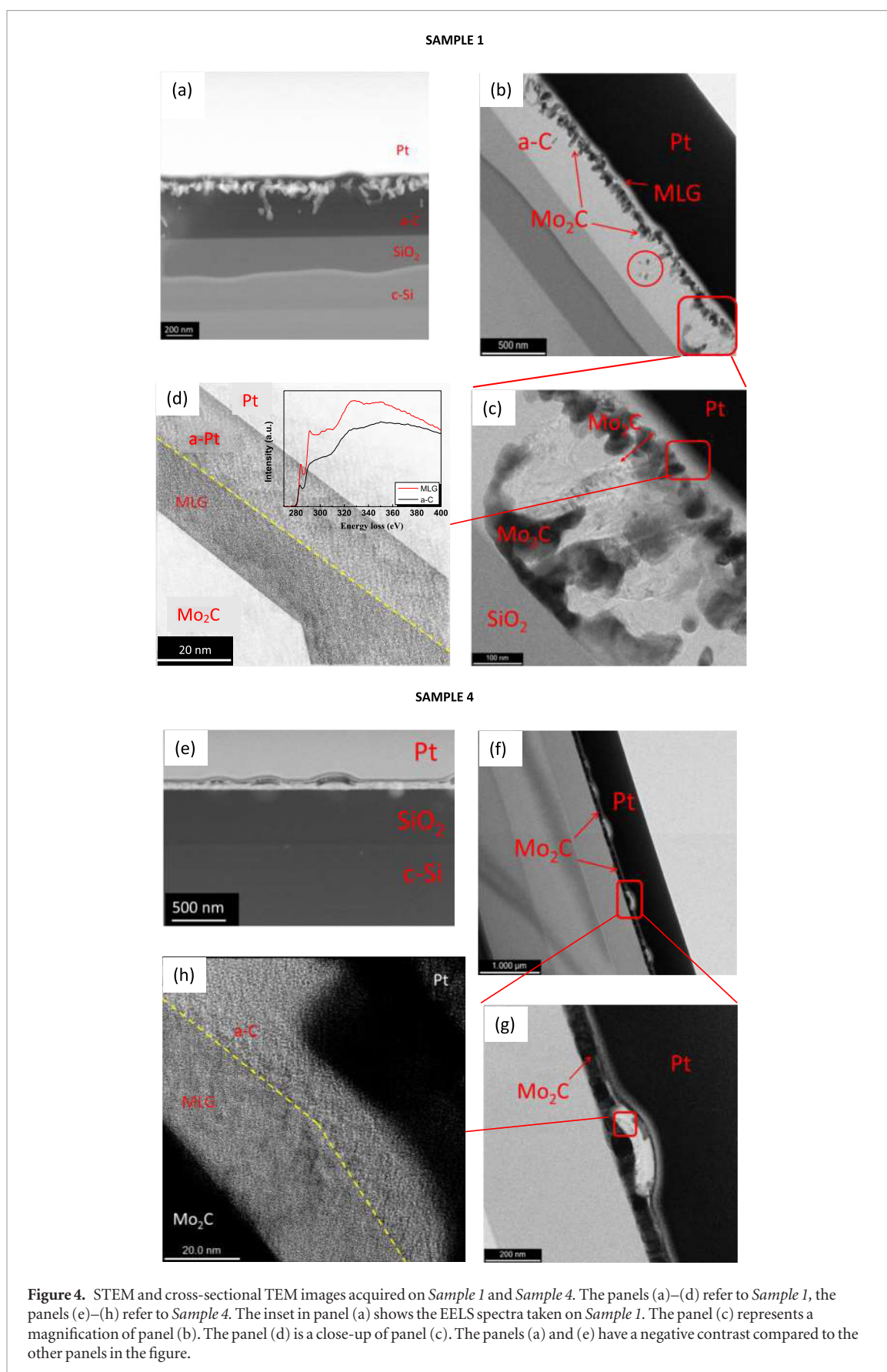
Sample 4 shows a similar behaviour as can be seen in figures 4(e)–(h). The STEM and TEM images show the modifications of the initial layers sketched in figure 2(d). Also in this sample, the diffusion of a-C into the Mo layer results in the Mo_2C formation (figure S1). For *Sample 4*, on top of the Mo_2C layer, a continuous film of MLG should be expected, as happens for *Sample 1*. Both figures 4(e) and (f) instead present agglomerated structures, which appear not homogenously distributed on the surface. A close-up (figure 4(g)) displays a bulge with a height of roughly 50–60 nm. The location of the bulges on top of the Mo_2C layer and the height comparable to the thickness of the initial a-C layer led to consider the bulges as agglomerations of the a-C film. These agglomerations originate from the anneal step. During the diffusion of C into the Mo and/or the segregation on top of the Mo_2C to form the MLG, the a-C film does not remain continuous. The film fragmentation is probably due to the low thickness of the initial a-C layer (40 nm) (figure S3).

Figure 4(h) shows the magnification of part of the bulge enclosed in the red frame in figure 4(g). The yellow dashed line (figure 4(h)) splits the bulge roughly into two parts. Below the line, the fringes are immediately on top of Mo_2C and the section of the layer is about 25 nm thick (~50 layers of graphene). Above the line, no ordered structures are recognized in the about 15 nm thick portion. The unorganized part might be the rest of the initial a-C layer which is not transformed into graphitic material. The thicknesses of Mo and a-C utilized for the experiments were comparable (table 1) and possibly not all a-C could diffuse into the Mo layer. The remaining a-C is left untransformed. The amorphous section in *Sample 4* clarifies the origin of the disordered area in *Sample 1*. In both samples, the thickness of the amorphous parts is comparable. In *Sample 4*, however, we have seen that the disordered part comes from the residues of a-C after the anneal. In fact, the Raman spectra point out those contributions. If the same contributions were present in *Sample 1*, the Raman spectra would have been analogously affected. The clear absence of any peak in the range $1100–1600$ cm^{-1} leads to conclude that the disordered part on *Sample 1* is formed after the growth process. The only possible source of amorphous material after the anneal step is therefore the Pt used for the lamella preparation.

To further understand the differences between *Sample 1* and *Sample 4*, we analyzed both samples by AFM. The two surfaces were distinctly different (figure 5).

Figure 5(a), as previously noticed in figure 4, exhibits a topography of the material different from that one observed in figure 5(b). The roughness value is about 6.8 nm whilst the substrate before the growth has a value approximately equal to 3.9 nm (see figure S4). The different values of roughness definitely confirm a significant modification induced by the anneal process.

Figure 4. STEM and cross-sectional TEM images acquired on *Sample 1* and *Sample 4.* The panels (a)–(d) refer to *Sample 1,* the panels (e)–(h) refer to *Sample 4.* The inset in panel (a) shows the EELS spectra taken on *Sample 1.* The panel (c) represents a magnification of panel (b). The panel (d) is a close-up of panel (c). The panels (a) and (e) have a negative contrast compared to the other panels in the figure.

As shown in figure 5(b), the material presents a roughness of about 20 nm which is in the same order of the Mo_2C crystals observed in the TEM images. AFM image (figure 5(b)) confirms that the thicker features are not homogenously distributed on the surface and have heights of about 50 nm, as indicated by the profile in the inset. These features correspond to the blob-like structures observed in the TEM.

The outcomes discussed so far and especially the TEM images shed light on the physics of the growth
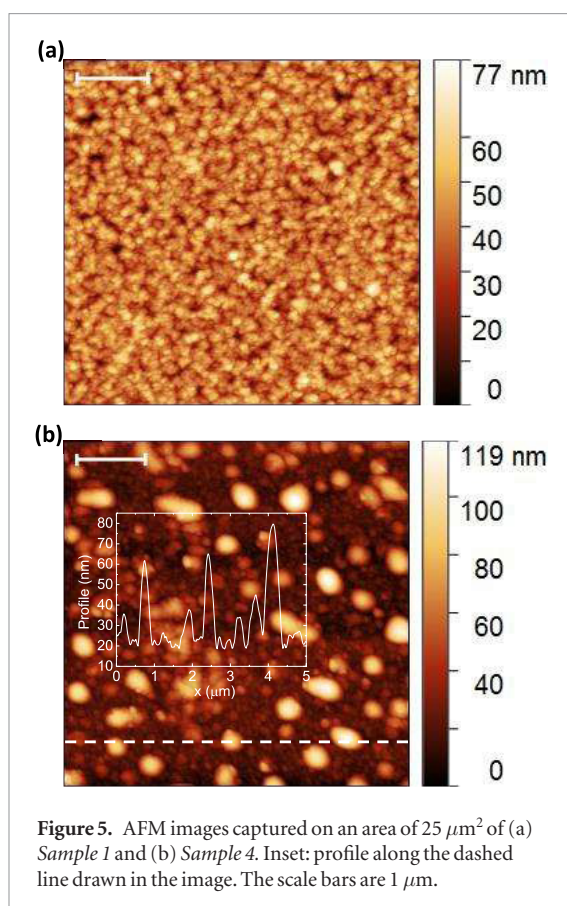
Figure 5. AFM images captured on an area of 25 μm^2 of (a) *Sample 1* and (b) *Sample 4*. Inset: profile along the dashed line drawn in the image. The scale bars are 1 μm.

mechanism. Assisted by the elevated temperature, a-C diffuses into the Mo layer, as basically shown in figures 4(a) and (b). Bulk Mo_2C is formed and the carbide serves as nucleating compound for the MLG precipitation on the top. As the solid a-C is the precursor both of the carbide and of the MLG, the amounts of precursor and catalyst matter. For instance, *Sample 1* and *Sample 2* have the same stack configurations but the thinner layer of a-C (40 nm) seems insufficient for the growth. All a-C is consumed for Mo_2C formation as witnessed by the Raman spectroscopy on *Sample 2* (figure 3(d)); nor graphitic nor a-C signal (figure 3(c)).

The proposed process is strengthened by comparing *Sample 3* with *Sample 4*, with an a-C layer thicknesses of 40 nm or 500 nm above the Mo film (50 nm, see table 1). *Sample 3* reveals only disordered hexagonal sp^2 structures. Some graphitic layers might be formed but the large thickness of a-C (500 nm) prevents the detection of any graphitic signal at the interface with Mo.

When the solid carbon source is 40 nm, such as in *Sample 4*, we observed a-C partially dissolved inside the Mo layer and partially untransformed, as previously discussed.

In order to further address the role of the annealing time in the growth process, *Recipes #1* was performed at two different times (indicated as *Recipe #2* and *Recipe #3* in table 2).

In figure 6 the average spectra obtained on the samples after these three recipes are compared. For sake of

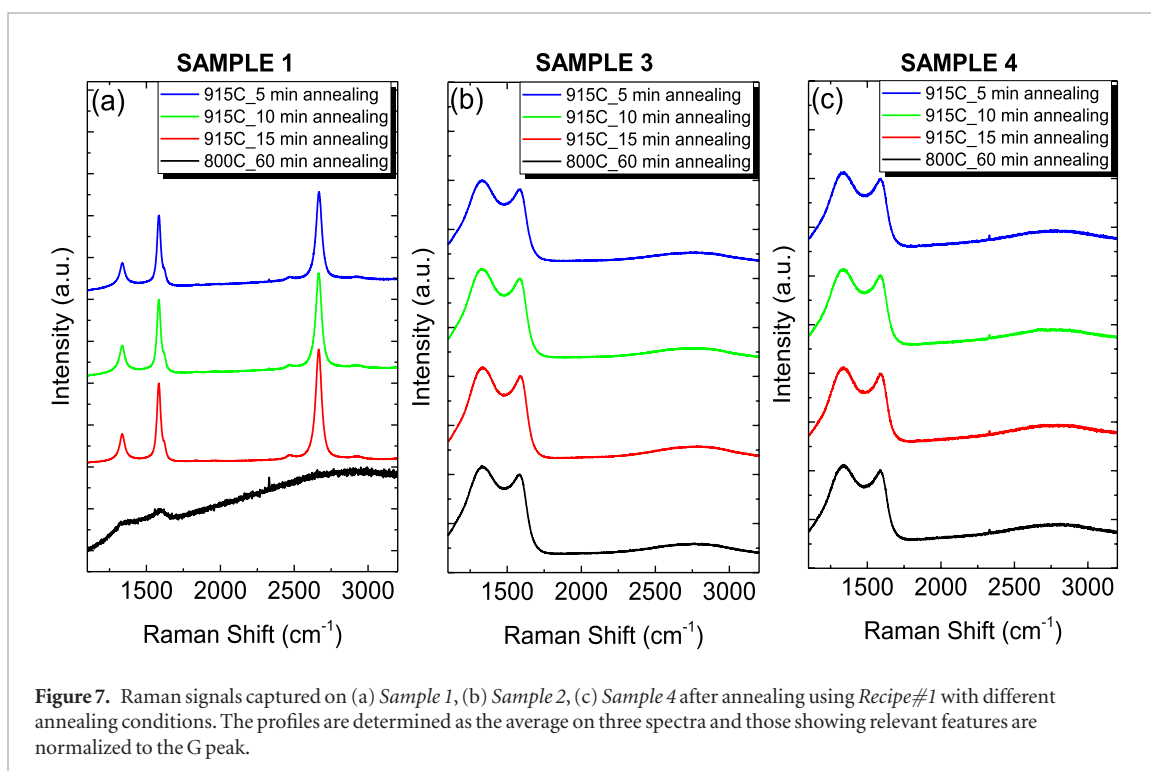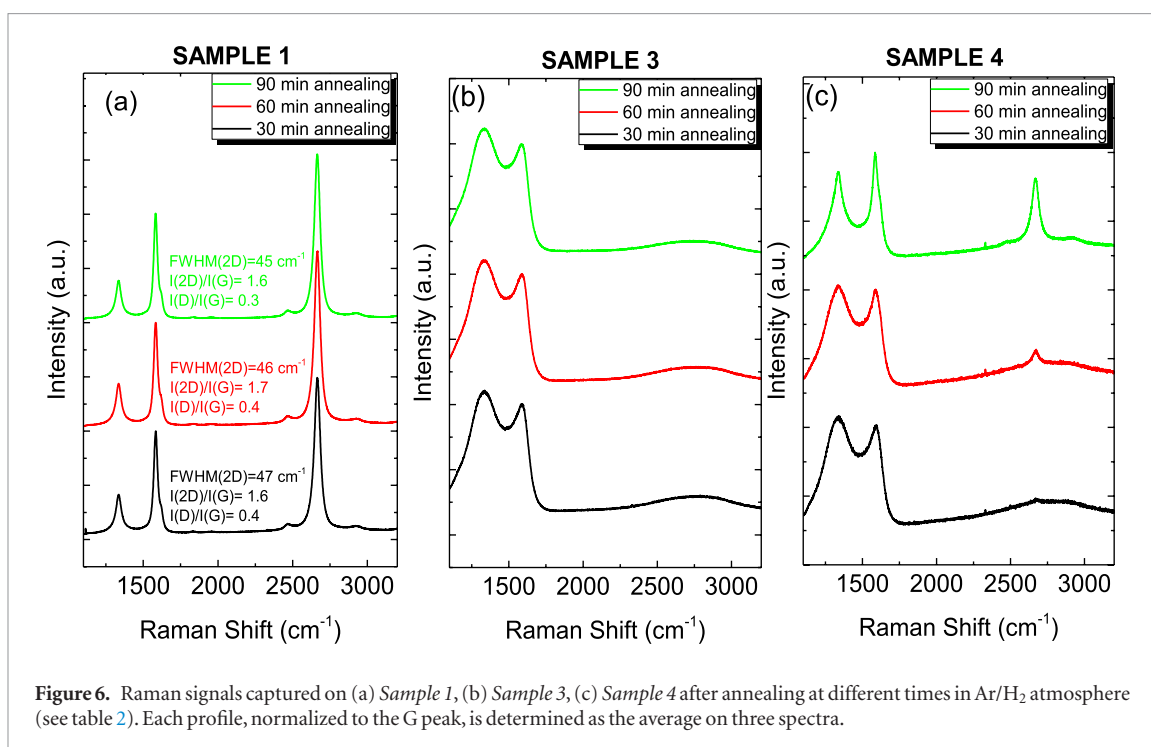clarity, *Sample 2* has not been reported, since no signal was detected on it, as previously shown.

For *Sample 1* and *Sample 3*, substantial differences as function of annealing time are not immediately detectable. The FWHM of the 2D peak and the intensity ratio between 2D and G peak ($I(2D)/I(G)$) are generally the useful parameters to first discriminate between SLG and few layer graphene (FLG) or MLG [25]. By fitting the 2D peak of *Sample 1* with a single Lorentzian, the FWHM(2D) equals 46 cm^{-1} proving the material to be MLG, as further settled by $I(2D)/I(G)$ roughly equal to 1.6 [30]. The ratio between the D and G peaks, $I(D)/I(G)$, is about 0.3 and demonstrates the high quality of the produced material, in close agreement with the findings obtained with the conventional CVD process [23, 25, 33].

It can be seen that a clear evolution of the Raman profile is observed for *Sample 1*. By increasing the annealing time, the material changes from disordered hexagonal sp^2 structures (black line) to MLG plus a-C (green line). The rise and shaping of the 2D band provides the most prominent indication of the graphitization. After 30 min of annealing, there is no presence of the 2D peak, which starts appearing after 60 min and it is well defined after 90 min growth. Decreasing the anneal time from 90 min down to 5 min on *Sample 1* still shows MLG growth with a quality similar to that reported in figure 6 for 90 min anneal. At a reduced anneal temperatures of 800 °C, we no longer observe any growth which is similar to our observations on CVD based MLG [34]. Figure 7 shows the comparison between the various anneal temperatures and times.

On *Sample 1*, the absence of any Raman fingerprint in panel figure 7(a) (black line) compared to the typical features present in figure 6(a) (red line) definitively proves that temperature value of 800 °C is not sufficient to grow MLG by the approach hereby presented. It is clear that both low temperature (800 °C) and shorter anneal time (5 min) produced the graphite clustering on *Sample 3* and *Sample 4* (figures 7(b) and (c)), as previously reported (see figure 3). Further investigations are required to explain if such temperature prevents Mo_2C formation or if the diffusion of C into Mo is too slow at 800 °C, requiring a significantly longer anneal time.

The experimental data attest that not only MLG can be directly obtained by annealing the a-C layer but also that an anneal time as short as 5 min is enough for the growth.

Atmospheres during the annealing process were varied to discover a possible effect of the gases on the growth mechanism. Since the etching power of H_2 on graphene during the conventional CVD process is well known, especially in presence of TMs [7], the mixture of Ar and H_2 used in the recipes so far described was replaced by only H_2 or Ar (last five recipes in table 2). The obtained results unclose that the growth

Figure 6. Raman signals captured on (a) *Sample 1*, (b) *Sample 3*, (c) *Sample 4* after annealing at different times in Ar/H$_2$ atmosphere (see table 2). Each profile, normalized to the G peak, is determined as the average on three spectra.

Figure 7. Raman signals captured on (a) *Sample 1*, (b) *Sample 2*, (c) *Sample 4* after annealing using *Recipe#1* with different annealing conditions. The profiles are determined as the average on three spectra and those showing relevant features are normalized to the G peak.

mechanism was not affected by the gas composition used (figure S5).

The growth mechanism worked for two configurations, i.e. a-C below and above Mo. In table 3 the features of the material presented in this paper are compared with those of material we synthesized in the Aixtron Black Magic Pro through the commonly used CVD process adopting the conventional hydrocarbon source [35–37]. In order to make the comparison more reliable with the growth by CVD, a growth time of 90 min has been selected, although we proved that there is no significant variance of the

Raman parameters by using the different annealing times.

The materials grown with the different recipes are remarkably similar. In particular, looking at *Sample 1* prepared through *Recipe #4*, the narrower 2D peak and the higher value of $I(2D)/I(G)$ with respect to *Recipe #1* indicate the synthesis of a slightly thinner material. We come to the same conclusion by comparing the values of FWHM(2D) and $I(2D)/I(G)$, especially those related to *Sample 1*, with the material we prepared by CVD. Our result suggests that the process with a-C is slower than the commonly used CVD, since in both processes

Table 3. Values of FWHM(2D), I(2D)/I(G) and I(D)/I(G) determined by the Raman spectra. These values are compared with those obtained by the standard CVD process.

	Recipe	FWHM (2D) (cm^{-1})	I(2D)/I(G)	I(D)/I(G)
Sample 1	*#1*	47	1.5	0.3
	#4	42	1.9	0.5
	#7	49	1.2	0.3
Sample 4	*#1*	59	1.0	—
	#4	63	1.0	—
	#7	62	1.0	—
Reference [35]	*Conventional CVD*	55	0.9	0.2

we have adopted the same growth time (90 min). Also for *Sample 4* the overall substantial equivalence with the conventional CVD process is underlined, showing a maximum variation of 15% of the FWHM(2D). For *Sample 4*, we did not take into account the ratio I(D)/I(G) for the comparison of the results. In fact I(D)/I(G) can be a misleading parameter since we have proved that for *Sample 4* the Raman spectrum contains contributions of both MLG and a-C residues.

The reported outcomes indicate that the growth through the annealing of solid phase carbon really has potential to provide 2D material having quality comparable and even higher than those grown by the CVD process adopting the usual hydrocarbon sources.

4. Conclusions

In this work, we have investigated the growth mechanism of MLG by thermal anneal of a solid a-C source in the presence of a Mo catalyst layer.

We proved that MLG growth happens with the catalyst layer sputtered either above or below an a-C layer. The growth mechanism consists of the diffusion of a-C inside the catalyst layer, followed by C segregation and MLG formation on top of Mo layer.

The highest quality of MLG, proved through Raman spectroscopy and cross-sectional TEM, was obtained with a 20 nm-thick Mo layer deposited on a 500 nm-thick a-C film. We found that the quality is at least as good as that obtained in conventional CVD with gaseous hydrocarbon sources, as can be seen from Raman results. We demonstrated that the minimum temperature to grow FLG is 915 °C. The annealing time was varied, discovering that MLG are achieved already after 5 min of anneal. We successfully demonstrated that the atmosphere during the anneal does not affect the material features. The presented findings provide a jolt towards a possible alternative for CVD based mechanisms.

Acknowledgments

ORCID iDs

Filiberto Ricciardella ⓘ https://orcid.org/0000-0002-9669-5649
Sten Vollebregt ⓘ https://orcid.org/0000-0001-6012-6180
Majid Ahmadi ⓘ https://orcid.org/0000-0003-2321-3060

References

[1] Soldano C, Mahmood A and Dujardin E 2010 *Carbon* **48** 2127
[2] Avouris P and Dimitrakopoulos C 2012 *Mater. Today* **15** 86
[3] Singh V, Joung D, Zhai L, Das S, Khondaker S I and Seal S 2011 *Prog. Mater. Sci.* **56** 1178
[4] Allen M J, Tung V C and Kaner R B 2010 *Chem. Rev.* **110** 132
[5] Ambrosi A, Chua C K, Bonanni A and Pumera M 2014 *Chem. Rev.* **114** 7150
[6] Mattevi C, Kim H and Chhowalla M 2011 *J. Mater. Chem.* **21** 3324
[7] Seah C M, Chai S P and Mohamed A R 2014 *Carbon* **70** 1
[8] Cabrero-Vilatela A, Weatherup R S, Braeuninger-Weimer P, Caneva S and Hofmann S 2016 *Nanoscale* **8** 2149
[9] Zhu Z, Zhan L, Wan W, Zhao Z, Shih T M and Cai W 2017 *Nanoscale* **9** 14804
[10] Zhu N L, Chen J, Cole M T and Milne W I 2017 *Proc. 19th Int. Conf. on Solid-State Sensors, Actuators and Microsystems* p 870
[11] Guermoune A, Chari T, Popescu F, Sabri S S, Guillemette J, Skulason H S, Szkopek T and Siaj M 2011 *Carbon* **49** 4204
[12] Li X *et al* 2009 *Science* **324** 1312
[13] Miyata Y, Kamon K, Ohashi K, Kitaura R, Yoshimura M and Shinohara H 2010 *Appl. Phys. Lett.* **96** 1
[14] Srivastava A, Galande C, Ci L, Song L, Rai C, Jariwala D, Kelly K F and Ajayan P M 2010 *Chem. Mater.* **22** 3457
[15] Kalita G, Sugiura T, Wakamatsu Y, Hirano R and Tanemura M 2014 *RSC Adv.* **4** 38450
[16] Hirano R, Matsubara K, Kalita G, Hayashi Y and Tanemura M 2012 *Nanoscale* **4** 7791
[17] Nakajima Y, Murata H, Saitoh N, Yoshizawa N, Suemasu T and Toko K 2018 *ACS Appl. Mater. Interfaces* **10** 41664
[18] Zhang Z, Mu S, Zhang B, Tao L, Huang S, Huang Y, Gao F and Zhao Y 2016 *J. Mater. Chem. A* **4** 2137
[19] Li W, Amiinu I S, Zhang B, Zhang C, Zhang Z, Zhu J, Liu J, Pu Z, Kou Z and Mu S 2018 *Carbon* **139** 1144
[20] Kou Z, Meng T, Guo B, Amiinu I S, Li W, Zhang J and Mu S 2017 *Adv. Funct. Mater.* **27** 1604904
[21] Peng T, Kou Z, Wu H and Mu S 2014 *Sci. Rep.* **4** 5494
[22] Peng T, Lv H, He D, Pan M and Mu S 2013 *Sci. Rep.* **3** 1148
[23] Ferrari A C and Robertson J 2000 *Phys. Rev.* B **61** 295
[24] Tuinstra F and Koenig J L 1970 *J. Chem. Phys.* **53** 1126
[25] Malard L M, Pimenta M A, Dresselhaus G and Dresselhaus M S 2009 *Phys. Rep.* **473** 51
[26] Rut'kov E V, Tontegode A Y, Usufov M M and Gall N R 1994 *Appl. Surf. Sci.* **78** 179
[27] Geng D, Zhao X, Chen Z, Sun W, Fu W, Chen J, Liu W, Zhou W and Loh K P 2017 *Adv. Mater.* **1700072** 1

[28] Flahaut E, Peigney A, Bacsa W S, Bacsa R R and Laurent C 2004 *J. Mater. Chem.* **14** 646

[29] Kanno H, Itakura M, Kuwano N, Masumori S, Miyao M and Sadoh T 2010 *Appl. Phys. Lett.* **96** 182101

[30] Ferrari A C *et al* 2006 *Phys. Rev. Lett.* **97** 187401

[31] Jang C W, Kim J H, Lee D H, Shin D H, Kim S, Choi S H, Hwang E and Elliman R G 2017 *Carbon* **118** 343

[32] Lin Y C, Teng P Y, Yeh C H, Koshino M, Chiu P W and Suenaga K 2015 *Nano Lett.* **15** 7408

[33] Ferrari A C and Basko D M 2013 *Nat. Nanotechnol.* **8** 235

[34] Ricciardella F, Vollebregt S, Polichetti T, Alfano B, Massera E and Sarro P M 2017 *Proceedings* **1** 445

[35] Ricciardella F, Vollebregt S, Polichetti T, Miscuglio M, Alfano B, Miglietta M L, Massera E, Di Francia G and Sarro P M 2017 *Nanoscale* **9** 6085

[36] Ricciardella F, Vollebregt S, Polichetti T, Alfano B, Massera E and Sarro P M 2016 *Proc. 2016 IEEE Sensors* (https://doi.org/10.1109/ICSENS.2016.7808638)

[37] Grachova Y, Vollebregt S, Lacaita A L and Sarro P M 2014 *Proc. Eng.* **87** 1501